PHYSICAL REVIEW A **86**, 012517 (2012)

Experimental observation and theoretical calculation of the diamagnetic spectrum of sodium Rydberg states

W. Gao,[1,2] H. F. Yang,[1,2] H. Cheng,[1,2] X. J. Liu,[1] and H. P. Liu[1,*]
[1]*State Key Laboratory of Magnetic Resonance and Atomic and Molecular Physics, Wuhan Institute of Physics and Mathematics, Chinese Academy of Sciences, Wuhan 430071, People's Republic of China*
[2]*Graduate School of the Chinese Academy of Sciences, Beijing 100049, People's Republic of China*

(Received 19 April 2012; published 31 July 2012)

We report diamagnetic spectra of sodium atoms observed in a strong magnetic field up to 3 T and compare them with theoretical calculations based on the formulation of an exact quantum-defect theory. We focus on one-photon absorption processes from the ground 3*s* state to the excited *np* Rydberg states whose magnetic quantum numbers are determined by the polarization of the laser field. The calculations employ *B*-spline basis expansion and the complex spatial coordinate rotation technique, and their results agree well with the observed ones when atomic core effects are appropriately taken into account. When graphed against magnetic field, level anticrossings and core-induced interaction of the *np* states provide clear signatures for studying the effects of quantum defect on the diamagnetic spectra.

DOI: 10.1103/PhysRevA.86.012517 PACS number(s): 32.30.Jc, 32.60.+i, 32.80.Ee, 31.15.−p

I. INTRODUCTION

Rydberg atoms in a magnetic field are an ideal system for studying the correspondence between classical nonintegrable dynamics and quantum chaos. In a pure magnetic field, the Rydberg atom system is rotationally symmetric about the direction of the magnetic field. Such a system provides a fascinating opportunity, especially when the diamagnetic term becomes comparable to the Coulomb potential. Numerous theoretical and experimental studies have been conducted on this system, for instance, the establishment and development of closed-orbit theory [1–4] and the confirmation of a quasi-Landau resonance region [5–12], as well as the existence of Rydberg progression. For lower-energy *np* states, the condition of comparable diamagnetic interaction with the Coulomb potential can only be satisfied in interstellar systems with an enormous magnetic-field strength such as in neutron stars [13]. For highly excited Rydberg states, however, a laboratory field strength of a few tesla can already give rise to favorable conditions [14–16] as the ratio of diamagnetic interaction to the binding energy scales as n^6B^2, where n is the principal quantum number and B is the magnetic field.

Even for hydrogenic atoms, the calculation of energy spectra in the regime we studied is by no means trivial due to the intensely distributed number of states and the presence of state mixing caused by the strong magnetic field. Several basis expansion methods, including the generalized Laguerre function basis [17], the Sturmian basis [18–21], the *B*-spline basis [22–25], and the discrete variable representation basis [26], were proposed and applied to the quantitative calculations of excited atoms in external fields. In the 1980s, Taylor and Clark performed an exact computation of the diamagnetic spectra for Rydberg states of a hydrogen atom using a large Sturmian basis [17,27]. Some consider *B*-splines derived from numerical analysis as one of the most efficient and accurate bases to calculate such spectra. It is also widely applied in quantum treatments of atomic systems [25].

The ionization potential of a sodium atom is lower compared to most other alkali atoms, easily accessible with pulsed lasers, making it one of the best candidates to investigate atomic diamagnetic effects in external fields. In 1978, Zimmerman *et al.* reported observing a group of sodium Rydberg states with $n = 27$–29 in up to 6-T magnetic fields and compared this result to their calculations carried out with numerical diagonalization using spherical basis states in the range $n = 25$–31 [28]. In 1980, Castro *et al.* discovered periodic resonance peaks in photoabsorption spectra of sodium atoms in a strong magnetic field [6], or the predicted quasi-Landau resonances (QLR) with a characteristic energy spacing of 1.5 $\hbar\omega_c$. Several other studies reported QLR of different periods using a commonly employed numerical method which combines the R matrix with quantum-defect theory [29] or directly diagonalizing the diamagnetic Hamiltonian in a basis constructed from model potential atomic eigenstates in the absence of magnetic field [30].

QLR is found to be insensitively dependent on the quantum defects of the atomic core, presumably because the concerned Rydberg states are of very high energy. For the lower-energy states, inclusion of the quantum defects is necessary to obtain an accurate calculation and to explain the fine structure embedded in the observed spectra in the presence of magnetic fields. The Coulombic potential energies for these states are comparable to the interaction strength with the external magnetic field, and additionally, the Rydberg electron is subjected to accumulative interactions from the atomic core, making the diamagnetic spectra of sodium atoms very complex and significantly different from that of the hydrogen atom. The quantum defects for sodium atoms have large values [31]:

$$\delta_s = 0.348, \ \ \delta_p = 0.855, \ \ \delta_d = 0.015.$$

This nonhydrogenic characters are well studied in the Stark map for sodium, lithium, and potassium alkali atoms with quantum-defect orbital theory [32]. The quantum defects for sodium atoms are nearly independent of energy for high Rydberg states, making it possible to refine theoretical calculations for exploring atomic properties inside a more

---

[*] liuhongping@wipm.ac.cn

complex environment, for example, in the discussion of the giant dipole moment in crossed electric and magnetic fields [33].

This paper reports our experimental investigation of the diamagnetic spectra of sodium atoms in static magnetic fields up to 3 T. We also carried out calculations for the corresponding measurement based on an exact quantum-defect theory, which incorporates quantum defects into the angular momentum quantum numbers in the centrifugal potential part. While the single-photon excitation couples the ground $3s$ to the excited np states, the diamagnetic interaction couples the adjacent $L \pm 2$ states, causing the np states to dominate the spectra. This latter selection rule simplifies the analysis of the spectrum and makes it possible to compare the theoretically calculated spectra to the experimental one thoroughly. Our theoretical calculation employs the complex coordinate rotation [22,29,31,34–37] and the B-spline basis expansion methods [22–25,38,39].

II. EXPERIMENT

Our experimental setup and the apparatus have been detailed previously [14,16]; therefore only a brief description is given here. A sodium atomic beam spouted from a resistance-heated oven travels to the interaction region after being collimated by two pinholes with diameters of about 2 mm. The beam direction is aligned along the magnetic field and is intersected perpendicularly by a pulse laser beam. Such a geometry avoids the motional Stark effect completely since the velocity component in the perpendicular plane of the magnetic field is negligible. The intense and stable magnetic field is generated by a superconducting magnet (Oxford Instruments), with a maximum magnetic field up to 4 T and a stability of better than 1 G in the present measurement.

The sodium atom is efficiently excited, through a one-photon transition into Rydberg states ($n \sim 30$), by a 10-ns pulsed laser in the intersection region. The laser wavelength is around 242 nm, and the linewidth is approximately 0.15 cm^{-1}. The laser pulse is produced by the dye laser system (Lambda Physik, Scanmate 2E) pumped by a Nd:YAG (Spectra Physics) laser and subsequently frequency doubled with a system-controlled barium borate crystal. The final excited states can be further selected by the polarizations of the laser beam tuned by the Soleil-Babinet compensator. The Rydberg atoms are ionized by a pair of electric grids of high voltage after passing through the interaction region, and the ion fragments are accelerated and efficiently detected by a two-layer microchannel plate situated at the end of the vacuum chamber. The ionization signal recorded by an oscilloscope (Tektronix TD1012) is downloaded into a personal computer for further processing. The data acquisition and the wavelength scanning are synchronized and controlled by integrated software running on a personal computer.

The one-photon excitation scheme avoids the pollution and complications from the intermediate excited states in two-step or multistep excitation configurations [40]. In an external field(s), nearby intermediate states can be affected, despite being nonresonant from the first-step excitation laser. Their excitations from the first-step photon absorption will complicate the final spectra.

III. THEORETICAL CALCULATION

To describe a single-electron atom inside a magnetic field, the nonrelativistic infinite-proton-mass Hamiltonian H for the Rydberg electron is adopted, which, in atomic units, takes the form [41]

$$H = \frac{p^2}{2} + V^{(c)}(r) + \frac{B}{2}L_z + \frac{B^2}{8}r^2 \sin^2\theta, \tag{1}$$

where $V^{(c)}(r)$ is the Coulomb potential including the effects of valence electron polarization for the core, B is the magnetic-field strength in atomic units, and θ is the polar angle of the Rydberg electron in spherical coordinates. $\frac{B}{2}L_z$ and $\frac{B^2}{8}r^2\sin^2\theta$ are, respectively, the paramagnetic and diamagnetic terms.

Solving the time-independent Schrödinger equation

$$H\psi = E\psi, \tag{2}$$

we can compute the transition probabilities corresponding to the experimental observations. Due to cylindrical symmetry along the magnetic-field direction, it is helpful to expand the eigen-wave-function in the truncated associated Legendre function basis,

$$\psi(r,\theta) = \sum_{l=|m|}^{l_{\max}} \frac{R_l(r)}{r} P_l^{|m|}(\theta), \tag{3}$$

where $P_l^{|m|}(\theta)$ is the normalized associated Legendre function and $R_l(r)$ is the expansion coefficient. l runs from $|m|$ to the truncated maximum value $l_{\max}$ with the boundary condition $R(r=0)=0$. In this basis, we can decompose the Hamiltonian in Eq. (1) into two parts:

$$H = H^{(0)} + V^{(\text{dia})}, \tag{4}$$

where $H^{(0)}$ is the diagonal part and $V^{(dia)}$ is the nondiagonal part, i.e., the diamagnetic term.

Rather than using the model potential rectified on the Coulomb potential [42,43] or the R-matrix method including the quantum defects implicitly [29,31,37], we employ an equivalent form by modifying the centrifugal potential [32],

$$V^{(c)}(r) = \frac{\lambda(\lambda+1) - l(l+1)}{2r^2} - \frac{1}{r}, \tag{5}$$

where $\lambda = l - \delta + \text{Int}(\delta)$ and the quantum defects are explicitly enclosed. Here $\text{Int}(\delta)$ is the rounded nearest-integer value of the quantum defect. An added benefit of this formula in Eq. (5) for the potential is that the Schrödinger equation has an analytic solution for its eigenfunctions [44–46]. We employ a reduced quantum defect,

$$\delta' = \delta - \text{Int}(\delta), \tag{6}$$

to quantify the real contribution of the quantum defect for a given angular momentum channel. In the following we will use δ rather than δ', i.e., ignore the prime. Obviously, the potential $V^{(c)}(r)$ is explicitly parameterized by the nonzero quantum defects.

In the radial direction, instead of expanding $R_l(r)$ in the quantum-defect orbital basis [47], in the present work, we will take the B-spline function as the basis, the main incentive being the Hamiltonian in the B-spline basis has a symmetric banded matrix form. This special matrix structure saves time in numerical diagonalization for its eigenvalues and eigenfunctions. In addition, radial coordinate rotation into the complex plane is employed in our calculation [22,29,31,34–37]. For pure magnetic field, the radial wave function of the system can be expanded in terms of the B-spline basis $\{B_0^k, B_1^k, \ldots, B_{N-1}^k\}$ according to

$$R_l(r) = \sum_{n=0}^{N-1} C_{nl} B_n^k(r), \tag{7}$$

where $B_n^k(r)$ is the nth B spline of order k defined in Refs. [25,38,39]. Both the Hamiltonian matrix and its wave functions are parameterized by the angular momentum quantum number l and the magnetic quantum number m; thus the wave function in Eq. (3) can be expanded completely in the defined basis sets. Substituting the Hamiltonian expressed in Eq. (1) and the wave function in Eq. (3) into Eq. (2), the Schrödinger equation is transformed into a general eigenvalue problem,

$$HC = ESC, \tag{8}$$

where E and C represent eigenvalues and their corresponding eigenvectors, respectively, H is the matrix form of the Hamiltonian in the B-spline basis, and S is the overlap matrix. Accurate matrix elements are obtained efficiently through the Gauss-Legendre integration scheme. A Lanczos algorithm for the general eigenproblem applied to the matrix equation can give the eigenvalue E and eigenvector C. In our case, the Schrödinger equation corresponding to Eq. (8) becomes

$$\sum_{n'l'} \left[H^{(0)}_{n,n'}\delta_{l,l'} + V^{(\mathrm{dia})}_{nl,n'l'}\right] C_{n'l'} = E \sum_{n'l'} S_{n,n'}\delta_{l,l'} C_{n'l'}. \tag{9}$$

The oscillator strength for the one-photon dipole transition from the initial state $|i\rangle$ to the final state $|f\rangle$ can be expressed as

$$c_{i\to f} = |\langle i\,|d|\, f\rangle|^2\,, \tag{10}$$

where d is the electric dipole operator. The signal detected is proportional to the population of the excited Rydberg state atoms resulting from photon absorptions. The absorption cross section $\sigma(E)$ from the initial state is then given by [29,31]

$$\sigma(E) \sim \mathrm{Im}\sum_n \frac{c_{i\to f}}{E_n - E}, \tag{11}$$

where E_n is the complex homologous energy eigenvalue and E is the resonant photon energy of the frequency-scanning laser pulse.

To make it sufficiently general and also adaptable for the calculation of the Stark spectrum by simply replacing the interaction term, we do not consider the symmetry of π parity in Eq. (3). The redundant calculation for states without applying the π symmetry in Eq. (3) does not actually contribute to the transitions since the corresponding oscillator strength does not satisfy the one-photon selection rule and is thus numerically equal to null in Eq. (10).

IV. RESULT AND DISCUSSION

In the experiment, the laser polarization can be rotated by the Soleil-Babinet compensator so that the sodium atoms are excited by the absorption of both π and σ photons. For a direct comparison with our experimental spectrum, the theoretically calculated spectrum in Eq. (11) is convoluted with a Gaussian function (a full width at half maximum $\Delta_G = 0.15$ cm^{-1}) to account for the Doppler broadening and the laser linewidth. They are displayed in upper frame, as shown in Figs. 1 and 2. The spectrum range we investigated extends from -180 to -25 cm^{-1}, and the magnetic field applied varies from $B = 2$ T to $B = 3$ T. The recorded spectra for the different situations are well resolved by carefully matching the laser wavelength and the applied magnetic fields.

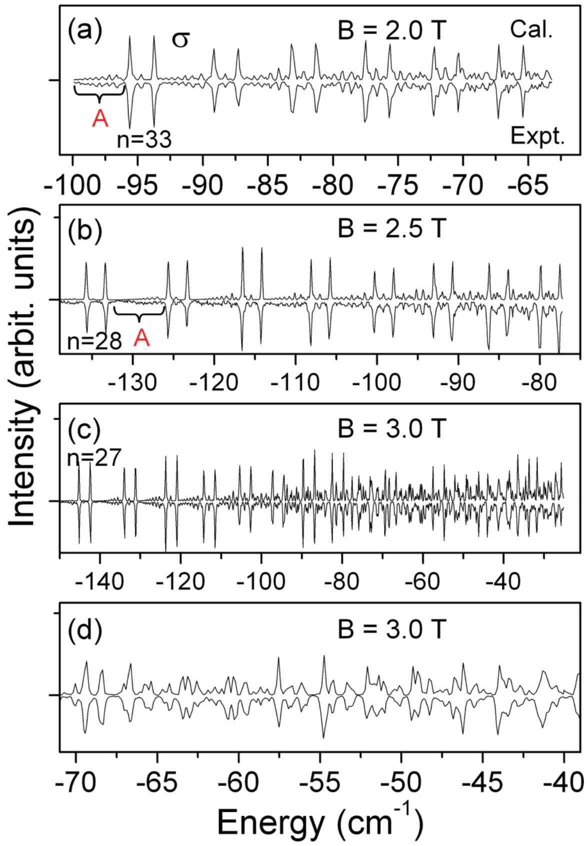

FIG. 1. (Color online) The calculated and observed diamagnetic spectra for the σ transitions. As the laser is linearly polarized perpendicular to the magnetic field, both σ^+ and σ^- transitions can occur. The two components are in coincidence if one of them is shifted by the paramagnetic energy difference $\Delta E = \frac{B}{2}\Delta m = B$ in atomic units. For example, this value is 1.87 cm^{-1} for (a). The split spectral lines within the same n-manifold are due to diamagnetic interaction at low energies such as those labeled A. Their spectra strengths are heavily suppressed in intensity due to the effect of significant quantum defects. Part of the spectrum in (c) is magnified in (d) for a better evaluation of the calculation.

Figure 1 shows the calculated and experimental σ spectra of sodium in magnetic fields from 2 to 3 T. As the laser is linearly polarized perpendicular to the magnetic field, both σ^+ and σ^- transitions occur simultaneously. The two components are in coincidence if one of them is shifted by the paramagnetic energy difference $\Delta E = \frac{B}{2}\Delta m = B$ in atomic units. In the calculation, we adopt the effective quantum-defect values from Ref. [31], taking $\delta_s = 0.348$, $\delta_p = -0.145$, $\delta_d = 0.015$, and $\delta_f = 0.002$. The quantum defects for higher angular momentum states are very small and thus are set equal to zero

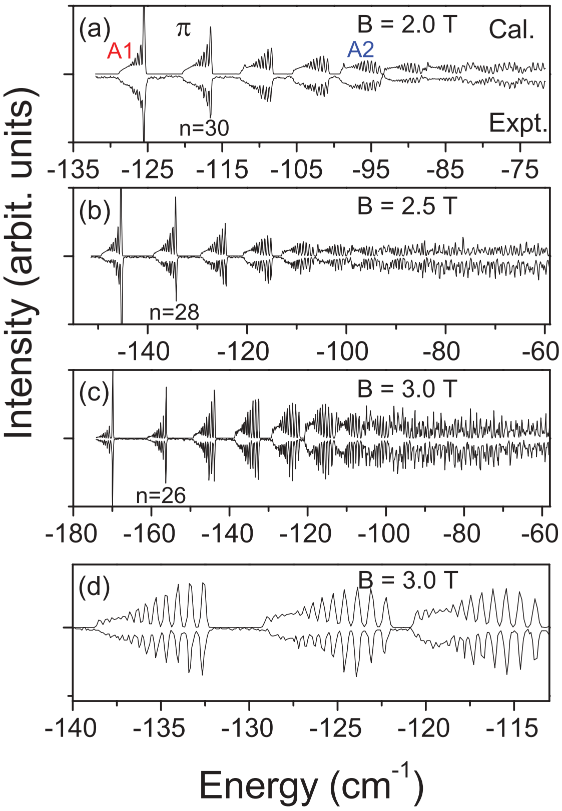

FIG. 2. (Color online) The calculated and observed spectra for the π transition. As the laser is linearly polarized along the magnetic field, only the π transition occurs. (a) reveals the spectral profile for n-manifolds at low and high energies. For example, at A1 and at A2, the spectra are very different. This spectral profile is similar to that of the hydrogen σ transition at A1. This abnormal spectral feature is attributed to the substantial quantum defect of the np states for sodium atoms, as explained in Fig. 3. Part of the spectrum in (c) is magnified in (d) for careful comparison.

in our calculation. From the observed spectra in Figs. 1(a) and 1(b), it seems that there are only spectral peaks corresponding to the principal quantum number n, and each peak appears as a pair. The split spectral lines within the same n-manifold due to the diamagnetic term are very weak and are labeled A. At higher energies above $E = -80\ \text{cm}^{-1}$, as in Fig. 1(c), we find these weak peaks become stronger with energy. In this limit the sodium atom behaves like a hydrogen atom in spectral character because of the large quantum defect of sodium for the np states, a point made clearer later. The calculated spectra are displayed in upper frame in Fig. 1. Selected regions of Fig. 1(c) are further enlarged in Fig. 1(d) for more convenient comparisons and better evaluations of the calculation. Taking the effects of the quantum defect into account, the calculation explains the experimental observations very well.

Following the σ spectrum, the π polarization transitions are also observed and calculated in the same magnetic-field strength as in Fig. 1. They are shown in Figs. 2(a)–2(c). At one magnetic-field strength, for example, at $B = 2.0$ T, below an energy of $E = -115\ \text{cm}^{-1}$, the spectrum is similar to that of the σ rather than the π transition of the hydrogen atom. For spectral lines in the same manifold n, intensities decay exponentially towards the low-energy direction, although this scaling does not persist into the end of the energy region, labeled A1 in Fig. 2(a). Above an energy of $E = -115\ \text{cm}^{-1}$, typically at the energies labeled A2, the spectral profiles in every manifold do not follow the exponential decay rule as those at low energies do. This spectral feature is also very different from that of barium atoms in magnetic fields [14], which behave closer to hydrogen atoms due to the negligible reduced quantum-defect values for its np states. This inversion of the spectral intensity distribution of the transition from π to σ reflects the prevailing competition of the core polarization effects induced quantum defect from the diamagnetic term. At higher energies, corresponding to the Rydberg electron at longer distances, the core polarization effect gradually trails off, and the spectrum will recover its profile and behave like hydrogen.

This abnormal spectral profile can be well understood in the numerical investigation of the calculated π spectrum by varying the quantum-defect values, as shown in Fig. 3. The calculation including quantum defects for all channels is taken as a reference, which is shown upwards. In Fig. 3(a), we notice that the variation of quantum defects of channels ns and nd does not change the spectrum at all. This is well understood by the matrix elements of the diamagnetic term. A prerequisite for nonzero elements is that the angular momentum quantum number satisfies $L' = L \pm 2$. For our case, the ns and nd states do not contribute to the excited states np. For most alkali and alkaline-earth atoms, the quantum defects of channels ns, np, and nd are quite substantial. If we investigate the diamagnetic spectrum by the transition to np states, we avoid taking the ns and nd states into account. This feature is very important to study atomic properties under complex external fields. The conclusion of the exclusion of ns and nd states

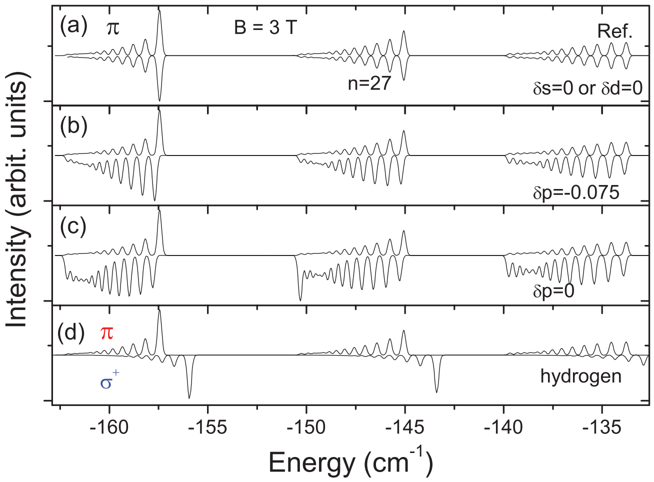

FIG. 3. (Color online) (a) The dependence of the calculated π transition spectrum on the quantum defects of channels ns, nd, and np. It is essentially independent of the quantum defects of channels ns and nd, although it remains sensitive to the quantum defect δ_p of channel np. (b) When δ_p decreases to $\delta p = -0.075$ and (c) when $\delta p = 0$, significant changes occur for the spectra. (d) For sodium atoms, quite counterintuitively, the heavily distorted π spectral profile resembles that of the hydrogen σ transition.

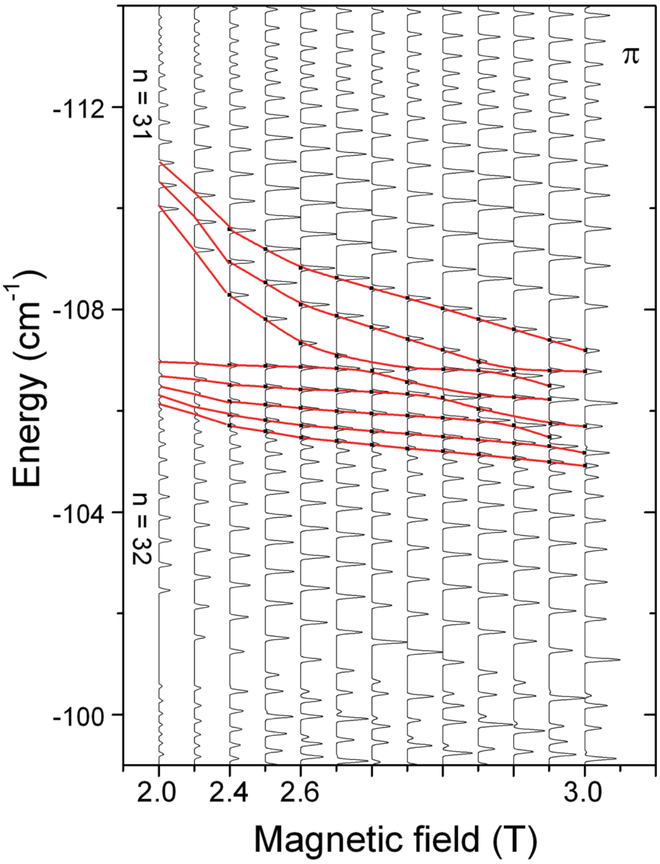

FIG. 4. (Color online) The calculated diamagnetic spectral map of the sodium π transition, showing a complex anticrossing with increasing magnetic fields. Note that the horizontal axis for the magnetic field is not linearly scaled in order to trace out the whole interior of the magnetic field. Between the labeled horizontal tick marks, the axis is linearly scaled.

can also be drawn by the application of symmetry to the atom in the magnetic field. On the contrary, from Figs. 3(b) and 3(c), we find that the calculated spectrum is heavily dependent on the quantum defects of channel np. When the quantum defect of np is decreased to $\delta p = -0.075$ and then $\delta p = 0$, significant changes occur for the spectral profiles. For sodium atoms, a larger value for δ_p keeps more high-energy states populated in one manifold, which counterintuitively resembles the hydrogen σ transition spectrum, as shown in Fig. 3(d).

Since the quantum defect of a sodium atom is substantial for the concerned one-photon transition from the ground state, we expect the diamagnetic spectrum will reveal its anticrossing properties on the energy levels. We calculate the diamagnetic spectrum of sodium in the small energy range -114 to about -110 cm^{-1} from $B = 2$ T to $B = 3$ T. The results are shown in Fig. 4, where we see the spectral lines from different n-manifolds are separated below $B = 2.6$ T, but at $B = 2.7$ T the spectral lines repel each other. Above $B = 2.7$ T, more complex and frequent anticrossings occur. We thus conclude that level anticrossing is a general feature for the diamagnetic-spectrum-associated states of nonzero quantum defects.

V. CONCLUSION

In summary, we observe the photoabsorption spectra of sodium in strong magnetic fields and calculate the corresponding theoretical spectrum. Using one-photon dipole coupling, only the np Rydberg states are excited, starting with the ground s states of alkali-metal atoms. Our method avoids the pollution from the intermediate states in the multistep excitation configuration and keeps the effects of the neighboring quantum channel away. Incorporating the quantum defects into the angular part of the centrifugal term, the calculation based on the B-spline expansion method and the complex coordinate rotation technique gives a satisfactory explanation for the experimental results. Due to the substantial quantum defect value for the np states, the π spectrum is heavily distorted and resembles the σ transition of a hydrogen atom. Our study proves that the diamagnetic map is an efficient method for understanding anticrossings between the concerned energy levels.

ACKNOWLEDGMENTS

This work is supported by the National Natural Science Foundation of China (Grants No. 11174329 and No. 91121005) and the 973 Program (Grant No. 2012CB922101).

---

[1] M. L. Du and J. B. Delos, Phys. Rev. A **38**, 1896 (1988).
[2] M. L. Du and J. B. Delos, Phys. Rev. A **38**, 1913 (1988).
[3] J. Gao, J. B. Delos, and M. Baruch, Phys. Rev. A **46**, 1449 (1992).
[4] J. Gao and J. B. Delos, Phys. Rev. A **46**, 1455 (1992).
[5] R. J. Fonck, D. H. Tracy, D. C. Wright, and F. S. Tomkins, Phys. Rev. Lett. **40**, 1366 (1978).
[6] J. C. Castro, M. L. Zimmerman, R. G. Hulet, D. Kleppner, and R. R. Freeman, Phys. Rev. Lett. **45**, 1780 (1980).
[7] A. Holle, G. Wiebusch, J. Main, B. Hager, H. Rottke, and K. H. Welge, Phys. Rev. Lett. **56**, 2594 (1986).
[8] J. Main, G. Wiebusch, A. Holle, and K. H. Welge, Phys. Rev. Lett. **57**, 2789 (1986).
[9] J. Main, A. Holle, G. Wiebusch, and K. H. Welge, Z. Phys. D **6**, 295 (1987).
[10] D. Wintgen and H. Friedrich, Phys. Rev. A **36**, 131 (1987).
[11] P. F. O'Mahony, Phys. Rev. Lett. **63**, 2653 (1989).
[12] W. Liu, X. He, and B. Li, Phys. Rev. A **47**, 2725 (1993).
[13] R. Cohen, J. Lodenqua, and M. Ruderman, Phys. Rev. Lett. **25**, 467 (1970).
[14] H. F. Yang, W. Gao, W. Quan, X. J. Liu, and H. P. Liu, Phys. Rev. A **85**, 032508 (2012).
[15] R. H. Garstang, Rep. Prog. Phys. **40**, 105 (1977).
[16] H. P. Liu, W. Quan, L. Shen, J. P. Connerade, and M. S. Zhan, Phys. Rev. A **76**, 013412 (2007).

[17] A. Holle, G. Wiebusch, J. Main, K. H. Welge, G. Zeller, G. Wunner, T. Ertl, and H. Ruder, Z. Phys. D **5**, 279 (1987).
[18] S. M. Susskind and R. V. Jensen, Phys. Rev. A **38**, 711 (1988).
[19] C. W. Clark and K. T. Taylor, J. Phys. B **15**, 1175 (1982).
[20] L. J. Dube and J. T. Broad, J. Phys. B **23**, 1711 (1990).
[21] L. J. Dube and J. T. Broad, J. Phys. B **22**, L503 (1989).
[22] J. Rao, W. Liu, and B. Li, Phys. Rev. A **50**, 1916 (1994).
[23] J. Sapirstein and W. R. Johnson, J. Phys. B **29**, 5213 (1996).
[24] E. Cormier and P. Lambropoulos, J. Phys. B **30**, 77 (1997).
[25] H. Bachau, E. Cormier, P. Decleva, J. E. Hansen, and F. Martin, Rep. Prog. Phys. **64**, 1815 (2001).
[26] T. P. Grozdanov, L. Andric, C. Manescu, and R. McCarroll, Phys. Rev. A **56**, 1865 (1997).
[27] C. W. Clark and K. T. Taylor, J. Phys. B **13**, L737 (1980).
[28] M. L. Zimmerman, J. C. Castro, and D. Kleppner, Phys. Rev. Lett. **40**, 1083 (1978).
[29] M. H. Halley, D. Delande, and K. T. Taylor, J. Phys. B **26**, 1775 (1993).
[30] W. Liu, X. He, and B. Li, Phys. Rev. A **47**, 2725 (1993).
[31] I. Seipp and K. T. Taylor, J. Phys. B **27**, 2785 (1994).
[32] I. Martin, J. Karwowski, C. Lavin, and G. H. F. Diercksen, Phys. Scr. **44**, 567 (1991).
[33] G. Raithel, M. Fauth, and H. Walther, Phys. Rev. A **47**, 419 (1993).
[34] J. Main and G. Wunner, Phys. Rev. Lett. **69**, 586 (1992).
[35] W. P. Reinhardt, Annu. Rev. Phys. Chem **33**, 223 (1982).
[36] D. Delande, K. T. Taylor, M. H. Halley, T. van der Veldt, W. Vassen, and W. Hogervorst, J. Phys. B **27**, 2771 (1994).
[37] M. H. Halley, D. Delande, and K. T. Taylor, J. Phys. B **25**, L525 (1992).
[38] T. K. Fang and T. N. Chang, Phys. Rev. A **76**, 012721 (2007).
[39] L. B. Zhao and P. C. Stancil, J. Phys. B **40**, 4347 (2007).
[40] E. Korevaar and M. G. Littman, J. Phys. B **16**, L437 (1983).
[41] J. Rao, B. Li, and K. T. Taylor, J. Phys. B **28**, 4715 (1995).
[42] Y. Li, Theor. Chem. Acc. **117**, 163 (2007).
[43] H. Y. Meng and T. Y. Shi, Commun. Theor. Phys. **52**, 333 (2009).
[44] J. M. Menéndez, I. Martín, and A. M. Velasco, J. Chem. Phys. **119**, 12926 (2003).
[45] I. Martin, A. C. Lavin, M. Velasco, M. O. Martin, J. Karwowski, and G. H. F. Diercksen, Chem. Phys. **202**, 307 (1996).
[46] J. M. Menéndez, I. Martín, and A. M. Velasco, Phys. Rev. A **74**, 043413 (2006).
[47] G. Simons, J. Chem. Phys. **60**, 645 (1974).